ELSEVIER

Journal of Nuclear Materials 297 (2001) 303–312

journal of nuclear materials

www.elsevier.com/locate/jnucmat

EXAFS/XANES studies of plutonium-loaded sodalite/glass waste forms

Michael K. Richmann *, Donald T. Reed, A. Jeremy Kropf, Scott B. Aase, Michele A. Lewis

Argonne National Laboratory, Chemical Technology Division, 9700 South Cass Avenue, Argonne, IL 60439, USA

Received 18 July 2000; accepted 23 May 2001

Abstract

A sodalite/glass ceramic waste form is being developed to immobilize highly radioactive nuclear wastes in chloride form, as part of an electrochemical cleanup process. Two types of simulated waste forms were studied: where the plutonium was alone in an LiCl/KCl matrix and where simulated fission-product elements were added representative of the electrometallurgical treatment process used to recover uranium from spent nuclear fuel also containing plutonium and a variety of fission products. Extended X-ray absorption fine structure spectroscopy (EXAFS) and X-ray absorption near-edge spectroscopy (XANES) studies were performed to determine the location, oxidation state, and particle size of the plutonium within these waste form samples. Plutonium was found to segregate as plutonium(IV) oxide with a crystallite size of at least 4.8 nm in the non-fission-element case and 1.3 nm with fission elements present. No plutonium was observed within the sodalite in the waste form made from the plutonium-loaded LiCl/KCl eutectic salt. Up to 35% of the plutonium in the waste form made from the plutonium-loaded simulated fission-product salt may be segregated with a heavy-element nearest neighbor other than plutonium or occluded internally within the sodalite lattice.

PACS: 61.10.Ht

1. Introduction

Sodalite/glass composite waste forms are being developed at Argonne National Laboratory (ANL) for the disposal of radioactive fission elements in salt from the electrometallurgical treatment of spent EBR-II nuclear reactor fuel [1,2]. The salt waste from the electrometallurgical process consists primarily of an LiCl/KCl eutectic salt (58 mol% LiCl) loaded with various other fission-product chloride salts. In addition, this salt also contains up to 2 mol% actinide chlorides, namely, uranium, plutonium, and neptunium chlorides. The salt from the treatment process is sorbed by zeolite 4A, which has an aluminosilicate cage structure of nominal composition $Na_{12}(AlSiO_4)_{12}$ and is known for its ability to contain or 'occlude' other species within the cage structure. The zeolite 4A, with its occluded fission-element salts, is mixed with glass and heated to high temperatures (1023–1123 K) and pressures (>96 500 kPa), i.e. expected process conditions, to convert the zeolite to a more thermodynamically stable sodalite form and consolidate the waste form. Primary considerations in this process are (1) the stability of the zeolite structure with respect to the various salts and (2) the fate of the fission elements in the resulting waste form. The objective of this work was to determine the fate of plutonium in this waste form via extended X-ray absorption fine structure (EXAFS) spectroscopy and X-ray absorption near-edge spectroscopy (XANES) synchrotron techniques [3]. Other techniques such as transmission electron microscopy (TEM) and scanning electron microscopy (SEM) can show crystal structure in great detail but do not have the ability to see the plutonium

* Corresponding author. Tel.: +1-630 252 7581; fax: +1-630 252 5246.

E-mail address: richmann@cmt.anl.gov (M.K. Richmann).

0022-3115/01/$ - see front matter
PII: S0022-3115(01)00637-7

within the sodalite cage structure. The EXAFS/XANES technique provides a unique means of determining the local environment of the plutonium where other techniques are effectively blind.

2. Experimental

2.1. Waste form preparation

The plutonium chloride (nominally K_2PuCl_5 at the prepared concentration, 35 wt% plutonium by assay) stock salt was produced by reacting bar stock 99.6% (remainder americium-241) pure plutonium metal (see Table 1 for isotopic breakdown) in an LiCl/KCl eutectic salt with a slightly substoichiometric amount of cadmium chloride ($CdCl_2$). The amount of cadmium chloride added was sufficient to react 99% of the plutonium metal present. This was done as the presence of a small amount of unreacted plutonium was preferable to the presence of $CdCl_2$. The mixture was heated to approximately 773 K to begin the reaction, then raised to 923 K to distill off the cadmium metal reaction product. The resulting K_2PuCl_5/LiCl/KCl salt was 35 wt% Pu and contained less than 100 ppm $CdCl_2$, as determined by chemical assay. When plutonium chloride alone was used, the stock salt was diluted with additional LiCl/KCl eutectic salt to produce a final salt that was 1.5 mol% plutonium. When simulated fission elements were present in the salt, the stock plutonium salt was diluted with a simulated fission-product salt (see Table 2 for the composition and Table 3 for the purity and source of the component salts) to produce a salt that was also 1.5 mol% plutonium. The stock plutonium salt and simulated fission-product salt were prepared in an argon atmosphere glovebox with oxygen levels typically at 0.2–0.4 ppm by weight and water levels less than 0.5 ppm. The oxygen/water atmosphere content expected under process conditions will likely be less rigorous so this level of purity provides a lower limit as well as a firm baseline for the analysis of this experiment.

The materials in Table 3 were used as received. Prior process experience has demonstrated that the purity of the stock chemicals was sufficient to rule out impurity contributions in the final result[1]. The simulated fission-product salt was transported to the glove box containing the plutonium stock salt in a hermetically sealed leak-checked vessel. The zeolite 4A powder was dried, assayed for water content (0.56 wt% by loss on ignition testing) and transferred in a hermetically sealed, leak-checked vessel.

The final salts for each case were milled in a Janke and Kunkel IKA A10 analytical mill at 12 000 rpm for three intervals of 1 min; the salt powder was scraped away from the mill walls between intervals. The milled salt was then added to sufficient zeolite 4A to produce a blended mixture that contained 13.04 wt% salt in the plutonium-only case and 12.01 wt% in the plutonium-

Table 1
Isotope and activity breakdown (in millions of becquerels) of plutonium metal used for chloride preparation

Isotope	Pu-238	Pu-239	Pu-240	Pu-241	Pu-242	Am-241
Wt%	0.055	87.414	11.318	0.568	0.230	0.386
Activity/4 g waste form specimen (MBq)	12.8	74.0	35.0	799	0.0122	16.8

Table 2
Simulated fission-product salt composition after plutonium chloride addition

Species	wt%	Species	wt%	Species	wt%	Species	wt%
LiCl–KCl	59.38	RbCl	0.281	CsCl	2.133	$PrCl_3$	0.979
$PuCl_3$	14.93	$SrCl_3$	0.861	$BaCl_2$	1.019	$NdCl_3$	3.315
NaCl	12.71	YCl_3	0.596	$LaCl_3$	1.039	$SmCl_3$	0.585
KBr	0.0196	KI	0.131	$CeCl_3$	1.983	$EuCl_3$	0.040

Table 3
Simulated fission-product salt specifications

Species	Mfr.	Purity (%)	Species	Mfr.	Purity (%)	Species	Mfr.	Purity (%)
LiCl–KCl	Lithcoa	99.9+	YCl_3	Alfa Aesar	99.9	$CeCl_3$	Alfa Aesar	99.5
NaCl	Alfa Aesar	99.9	KI	Alfa Aesar	99.988	$PrCl_3$	Alfa Aesar	99.9
KBr	Alfa Aesar	99.9	CsCl	Alfa Aesar	99	$NdCl_3$	Alfa Aesar	99.9
RbCl	Acros	99+	$BaCl_2$	Alfa Aesar	99.998	$SmCl_3$	Aldrich	99.9
$SrCl_3$	Alfa Aesar	95	$LaCl_3$	Aldrich	99.9	$EuCl_3$	Acros	99.9

with-fission-element case. These loadings corresponded to a loading of 3.8 chlorides per zeolite unit cell, which is slightly below the theoretical maximum loading of four chlorides per unit cell attainable in sodalite [4]. The mixture was placed in an alumina crucible at 773 K and mechanically stirred; the mixture was scraped away from the crucible walls and corners at 1.5-h intervals. The mixing was done in two separate periods of 8 h stirring, 16 h resting. The blended zeolite/salt mixture was then examined via X-ray diffraction (XRD); it had a clean zeolite 4A pattern with small traces of LiCl and PuO_2 visible as well. This determination was aided by the fact that plutonium is a high-Z atomic number element and the matrix was, on average, of low-Z composition.

The zeolite/salt mixture was mixed with glass powder (See Table 4 for specifications) in a 3:1 weight ratio to make a 4-g sample for pressing. The 4-g powder sample was placed within a graphite die (1-in. ID) of nominal 99.95 wt% purity and pressed using a uniaxial press to a cold starting pressure of 17 200 kPa. The press was located in the floor-mounted glove box furnace well in the glove box used to prepare the salt mixtures, and the sample was heated at a rate of 1.4 K/min. The pressure was increased on the die at a rate such that the pressure reached its limiting value of 57 900 kPa when the press temperature reached 923 K. At this point, no further pressure was added and was, in fact, allowed to freely decrease as the temperature climbed to the final value of 1023 K. This protocol prevented the sample from becoming fluid enough to squeeze out between the die and piston walls. The sample was nominally held at 1023 K for 3 h, and the furnace was then turned off to cool overnight. At this point, the pressure reading was typically ~13 800 kPa. The average rate of temperature drop was 37 K per hour. These process conditions do not quite match those of the ANL-W process but do serve as a representative case given equipment constraints. The following day, the press was removed from the furnace well, and the sample was extracted from the graphite die. Samples for characterization were taken from the interior of the sample to avoid any issues with incorporation of graphite although no incorporation was physically observed. XRD characterization of a portion of the resultant ceramic composite indicated complete conversion to sodalite, with PuO_2 being a small component.

Small bulk pieces of this material were then mounted using a styrene epoxy in a once through nitrogen glove box with sub-ppm water content to maintain their original anhydrous state. The hydrated samples were exposed to room atmosphere of 50% average relative humidity for 96 h and then mounted in the same manner as the anhydrous case. The samples were then covered with Kapton for additional containment and transported to the Materials Research Collaborative Access Team (MRCAT) insertion device beamline (Sector 10) at the Advanced Photon Source (APS) for EXAFS/XANES analysis. The samples created from the K_2PuCl_5/LiCl/KCl stock will be referred to as ES-sodalite, while the samples created from the simulated fission product salt will be referred to as DS-sodalite.

Table 4
Specifications of glass powder used in zeolite/glass mixture

Species	SiO_2	B_2O_3	Al_2O_3	Na_2O	K_2O
Wt%	66.5	19.1	6.8	7.1	0.5

2.2. EXAFS/XANES standards

The following representative plutonium-containing standards were used in the course of this investigation: $Pu(III)F_3$, $Pu(IV)O_2$, $NaPu(V)O_2CO_3$ and $Ba_3Pu(VI)O_6$. The standards were all fine powders dispersed on Kapton tape and encapsulated in a chlorine-free styrene matrix. Since the actinide L edges are all at fairly high energy (>15 keV), the encapsulation matrix is essentially transparent.

The four types of plutonium solids were synthesized using standard methods with Pu-242 (50% purity by activity, >99% purity by isotope). Pu-238 and Pu-241 accounted for the vast majority of the remaining sample activity not due to Pu-242. The PuF_3 was synthesized by oxidizing Pu to Pu(III), taking the product to dryness in hydrobromic acid, adding fluoride after dissolution in water, and precipitating. The plutonium oxide was made from high-purity oxide stock, which was provided by Oak Ridge National Laboratory. It was high-fired in air to ~1273 K. The $NaPuO_2CO_3$ was precipitated from Pu(V) stock, which was made by electrolytic reduction of Pu(VI), by titrating with sodium carbonate solution to pH ~ 7. The Ba_3PuO_6 was used as received from stock previously synthesized at ANL. The standards were characterized optically using a Varian CARY 5E spectrometer.

3. Synchrotron characteristics

The APS synchrotron ring operates at 7 GeV, 50–100 mA. The undulator (model A) used at the MRCAT beamline [5] was tapered and scanned. The monochromator is a cryogenic double Si(1 1 1) crystal operated in pseudo-channel-cut mode, with a thin web first crystal. At the energies used in this experiment, the beam position is essentially fixed. Harmonic rejection was accomplished using a rhodium coated mirror. Four detectors were used with the following characteristics: I_0 filled with 15% Ar/85% N_2, I_t filled with 15% Ar/85% N_2, I_f filled with argon gas, and I_{ref} filled with nitrogen. The energy resolution of the system was ~4 eV at 18 keV; the resolution was estimated from a measurement

of the rocking curve width and vertical slit size. The beam size was 1 mm horizontal × 0.7 mm vertical.

4. Results and discussion

4.1. Thermodynamic considerations

Of primary concern in these experiments is the fate of the plutonium. Thermodynamic calculations using HSC [6,7] indicate probable reaction paths at process temperature and, therefore, the most likely species to be found in the experiment. Nepheline was used as a stand-in for zeolite 4A in the following equations due to the lack of the necessary thermodynamic data; it is possible that other reactions could occur with the zeolite as well:

$$4PuCl_3(s) + 8H_2O(g) \rightarrow 4PuO_2(s) + 12HCl(g) + 2H_2(g)$$
$$\Delta_r G^\circ_{773\ K} = -9.20\ kJ/mol;\ \Delta_r H^\circ_{773\ K} = 115\ kJ/mol, \quad (1)$$

$$4PuCl_3(s) + 4H_2O(g) \rightarrow 4PuOCl(s) + 8HCl(g)$$
$$\Delta_r G^\circ_{773\ K} = -18.7\ kJ/mol;\ \Delta_r H^\circ_{773\ K} = 89.1\ kJ/mol, \quad (2)$$

$$4PuCl_3(s) + 12NaAlSiO_4(s) \rightarrow 4PuO_2(s) + 12NaCl(s) + Si(s) + 6Al_2O_3(s) + 11SiO_2(s)$$
$$\Delta_r G^\circ_{773\ K} = -21.8\ kJ/mol;\ \Delta_r H^\circ_{773\ K} = -52.1\ kJ/mol, \quad (3)$$

$$4PuCl_3(s) + 8NaAlSiO_4(s) \rightarrow 4PuOCl(s) + 8NaCl(s) + 4Al_2O_3(s) + 8SiO_2(s)$$
$$\Delta_r G^\circ_{773\ K} = -87.1\ kJ/mol;\ \Delta_r H^\circ_{773\ K} = -91.7\ kJ/mol, \quad (4)$$

where 773 K was chosen as the reference temperature since the zeolite contacts the salt at this approximately this temperature for an extended period of time prior to the cooling, mixing and subsequent raising of temperature to produce the ceramic. In both cases, either the plutonium oxide or more likely the oxychloride is predicted to be the reaction product, whether the pathway is from reaction with water present in the system or attack upon the zeolite structure. XRD results do not display any zeolite decomposition products, which may belie the accuracy of using nepheline as a zeolite substitute and/or indicate that kinetics play a prime role in this system. In addition, other analytical techniques (XRD, SEM, TEM, mass-spectrometry) have shown that zeolite structural attack does not occur [8], making reactions (1) and (2) the primary focus. This will be discussed in more detail in the following analysis.

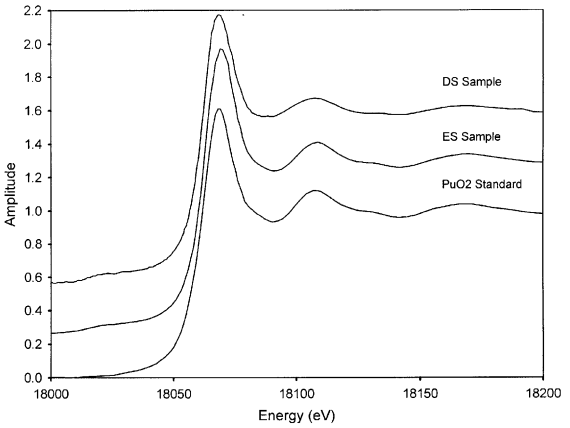

Fig. 1. XANES data for plutonium L_{III} edge in case using the plutonium bearing LiCl/KCl salt compared to Pu(IV) standard. The small rise in the waste form data at 18 020 eV is a zirconium contribution from the glass in the system.

5. XANES results

XANES data were acquired to determine the plutonium oxidation state. The spectra for the $PuCl_3$/LiCl/KCl (ES-sodalite) samples were found to be nearly identical to the $Pu(IV)O_2$ reference spectrum (see Fig. 1). However, the spectra for the plutonium-loaded simulated-fission-product salt case (DS-sodalite) exhibit subtle differences when compared to the ES-sodalite. These differences can be interpreted in terms of a difference in particle size as well as the presence of an additional phase.

6. EXAFS results

EXAFS data were acquired to determine the local environment of a particular element. Fig. 2 displays the EXAFS χ-space data for a number of representative data sets. This figure shows that all of the unknown cases are similar to the plutonium(IV) oxide standard. Given that the XRD work on the samples before EXAFS analysis indicated the presence of PuO_2, this was not unexpected. The ES-sodalite spectrum is nearly identical, while the DS-sodalite spectrum has some differences, consistent with the observations made for the XANES spectra. The Fourier transforms of the EXAFS data (see Fig. 3) clearly indicate the similarity of all of the specimens to $Pu(IV)O_2$.

Further comparison to the experimental data sets was accomplished using known crystallographic data input to FEFF8 [9,10]/FEFFIT [11]. These utilities can take crystallographic data and generate EXAFS data for comparison against the experimental data. Verification of the performance of the various programs (FEFF8,

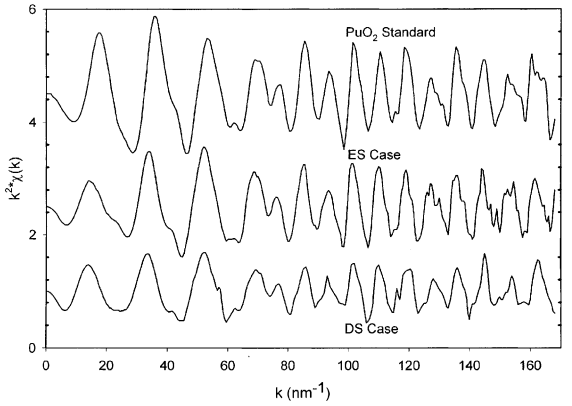

Fig. 2. Comparison of $k^2\chi$-space data for the various unknowns against the plutonium dioxide standard.

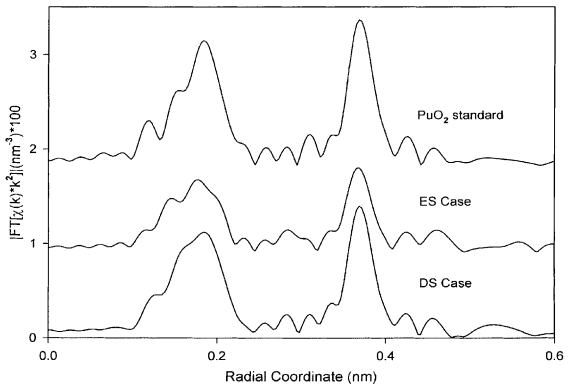

Fig. 3. Comparison of radial shell data for the cases in Fig. 2 with k-range = 28–155 nm^{-1}, dk = 10 nm^{-1}, and k^2 weighting.

FEFFIT) was checked by generating the EXAFS for PuO_2 from the known crystallographic data and comparing it against the experimental data; it was found to have excellent agreement (see Figs. 4 and 5).

The samples were first fit using WinXAS [12] in order to compare them to the experimental PuO_2 reference. These results are shown in Table 5. Comparison to an experimental reference provided results that are more accurate for the coordination numbers for Pu–O and Pu–Pu neighbors than fitting to ab initio calculations. However, for the DS sample, it was apparent that another phase was present. Therefore, the DS data were also fit to ab initio calculations in order to determine the magnitude of the effect of the second phase.

Other chemical species were also considered, even though thermodynamics suggests that they are not active species in this situation, using crystallographic data to compare to the samples: Pu_2O_3, PuOCl, $PuCl_3$, K_2PuCl_5, and K_2PuCl_6 (see Figs. 6 and 7).

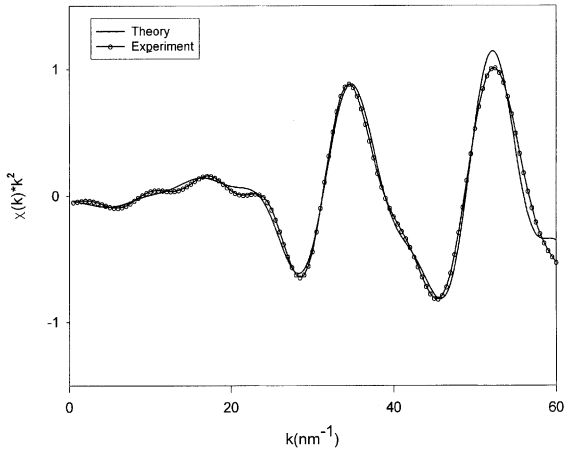

Fig. 4. Comparison of fit to isolated first and second shell data for the inverse transform isolated first and second shells (three shells used in fit) from the plutonium dioxide standard using k = 28–135 nm^{-1}, dk = 10 nm^{-1}, k^2 weighting and r = 0.135–0.430 nm.

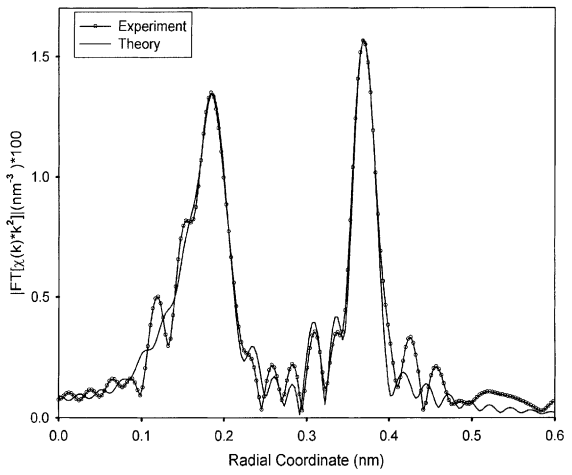

Fig. 5. Comparison of fit to experimental Fourier transform data for the plutonium dioxide standard using r = 0.135–0.430 nm.

Pu_2O_3 yielded the most similar simulation, since the Pu near-neighbor distances are similar [13,14]. Nonetheless, the amplitude of the Pu–O paths and the split Pu–Pu shell failed to match the samples. PuOCl, one of the potential phases predicted by thermodynamics failed to match the data [13]. Also, although the Pu–O and Pu–Pu are somewhat similar, the Pu–Cl path, with a peak in the Fourier transform at ca. 0.27 nm, is entirely absent in the samples. The plutonium chloride[15] and potassium plutonium chloride [16,17] species also were a poor match to the experimental Pu–Pu distances.

Table 5
Plutonium fitting results from experimental references and ab initio calculations using $k = 28$–$135\ \mathrm{nm}^{-1}$, $r = 0.13$–0.43 nm and $\mathrm{d}k = 10\ \mathrm{nm}^{-1}$

Sample	Path	N	R (nm)	$\sigma^2(\times 10^{-5}\ \mathrm{nm}^2)$	Min. avg. particle size (nm)
$Pu(IV)O_2$	Pu–O	8[a]	2.344[a]	5.0[b]	
	Pu–Pu	12[a]	3. 833[a]	2.9[b]	
ES-sodalite	Pu–O	7.4 ± 0.4[c]	2.347 ± 0.007[c]	5.0 ± 1.0	4.6(+6.0/−1.9)
	Pu–Pu	10.6 ± 0.4[c]	3.838 ± 0.006[c]	2.9 ± 0.5	4.8(+1.9/−1.1)
DS-sodalite	Pu–O	5.2 ± 0.3[c]	2.336 ± 0.008[c]	4.6 ± 1.0[c]	1.4 ± 0.2
	Pu–Pu[d]	0.7 ± 0.3[b]	3.03 ± 0.05[b]	2.4 ± 0.6[e]	
	Pu–Pu	6.2 ± 0.4[c]	3.821 ± 0.008[c]	2.4 ± 0.6[c]	1.3 ± 0.15[f]

[a] Crystallographic data.
[b] Fitting to ab initio calculations.
[c] Fitting to experimental reference.
[d] Denotes a surrogate used to model the plutonium-heavy nearest neighbor path.
[e] Fixed value.
[f] Assuming 15% plutonium in an unknown heavy element phase.

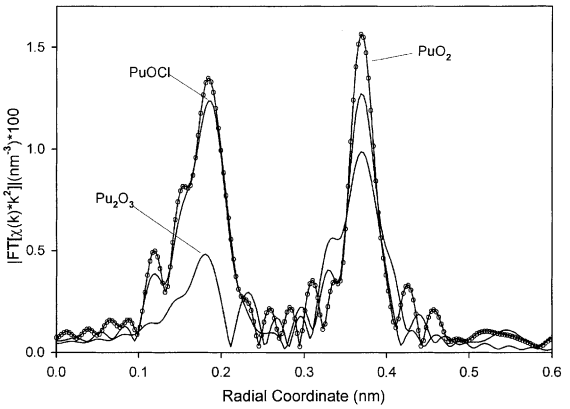

Fig. 6. Comparison of PuO_2, Pu_2O_3 and PuOCl standards using $k = 28$–$135\ \mathrm{nm}^{-1}$, $\mathrm{d}k = 10\ \mathrm{nm}^{-1}, k^2$ weighting and $r = 0.135$–0.430 nm.

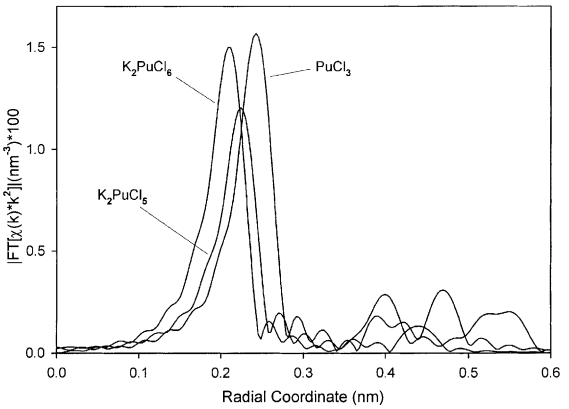

Fig. 7. Comparison of $PuCl_2$, K_2PuCl_5 and (K_2PuCl_6 standards using $k = 28 - 135\ \mathrm{nm}^{-1}$, $\mathrm{d}k = 10\ \mathrm{nm}^{-1}$, k^2 weighting and $r = 0.135$–0.430 nm.

7. Particle sizes

One of the measurable parameters in the EXAFS signal is the coordination number (N) of the near-neighbor elements. If the absorbing atom is located in a known single phase and the particles are predominately similar in size, then the coordination number can be used to estimate a particle size for small particles. There is some debate as to the accuracy of this determination, due to the assumed changes in the vibration modes of small particles, for which surface effects are more important than for larger particles [18,19]. Due to anharmonic effects, disorder at the surface is believed to reduce the measured coordination number below its actual value. The result is that an estimate of the average particle size from EXAFS should always underestimate the true particle size. If the plutonium resides primarily in small particles in the waste form then the coordination number will give a reliable lower limit to the average particle size.

A systematic study of particle sizes in copper supported catalysts demonstrated the decrease in the coordination number measured by EXAFS compared to the true coordination number [18]. If the assumption is made that the Debye–Waller factor (DWF) for a small particle is the same as for the bulk material, significant deviations are observed for particles smaller than 7.0 nm, becoming worse for smaller particles and at elevated temperatures. Deviations as large as 20% in the coordination number were observed at room temperature in 1.7 nm copper particles. By allowing the DWF to be an adjustable parameter, the coordination number error was reduced to only about 5% for the 1.7 nm particle, which still translates into an underestimate of the particle size by as much as 25%, due to the non-linear dependence of the copper particle size on the coordination number. Due to this substantial effect, the DWF was

used as an adjustable parameter for the plutonium specimen characterization/fitting reported here.

Unexpectedly though, the best fit DWF value in this work was somewhat lower than the bulk value, albeit within the measurement error. However, the DWF is already quite small for the Pu–Pu path ($\sim 2.9 \times 10^{-5}$ nm^2). Since the thermal vibration amplitude is low to begin with, anharmonic vibrations would be expected to have a minimal effect on the measured coordination number – specifically, a smaller effect than for the small copper particles described by Clausen. In the DS samples, which exhibit the smaller particle size, the Pu–Pu distance is slightly lower than that of the bulk material, indicative of anharmonic vibration modes [18]. Therefore, it is likely that the EXAFS measurements underestimate the true particle size for these samples. Such is not the case for the ES samples and N_{Pu-Pu}, as measured, should be very close to the actual value.

In the various cases discussed thus far, XRD and TEM measurements demonstrated the existence of PuO_2 particles in the sample. XRD measurements are insensitive to very small particles, especially in the presence of larger particles. As such, in this work, the XRD technique was used primarily as an indicator of the species present within the sample. In addition, neither XRD nor TEM can definitively determine whether plutonium is occluded within the sodalite cage, a key consideration when evaluating the material as a waste form. The EXAFS signal, on the other hand, is an average over all of the plutonium within the sample. Thus, the existence of nanoscale phases and occluded plutonium can be inferred from the data, if present in large enough quantities. In many cases, the coordination number can be accurate to about 5%, especially when comparing like samples. Therefore, the existence of non-PuO_2-like phases may be detectable above the 5% level.

Several limiting cases are considered below with respect to their signature in the data:

(1) *Large PuO_2 particles only* (>8 nm). The EXAFS data in this case would essentially match the bulk PuO_2 data, with coordination numbers and radial distances matching the bulk material. XRD patterns would have sharp diffraction lines with the line width depending on the particle size.

(2) *Small PuO_2 particles in a tight distribution about one size* (<8 nm). The EXAFS data in this case would have a reduced coordination number for the next-nearest-neighbor plutonium path, N_{Pu-Pu}. For small enough particles, N_{Pu-O} would also be reduced. XRD patterns would show a significantly broadened line width corresponding to the smaller particle size until at some small size the diffraction line would be too broadened to be visible. Fig. 8 shows N_{Pu-O} and N_{Pu-Pu} as a function of particle size.

(3) *Plutonium only found inside the cage structure of the sodalite*. The EXAFS data of a plutonium ion inside

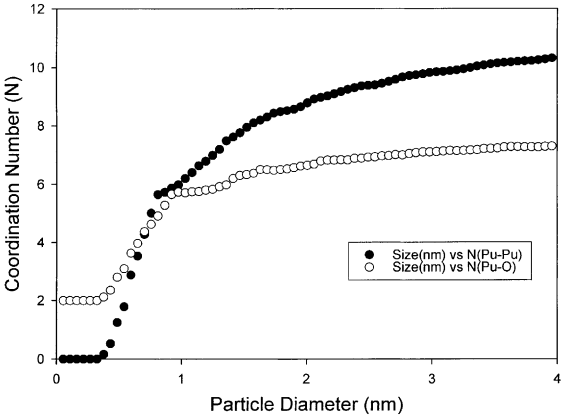

Fig. 8. Plot of coordination number versus true particle size for Pu–Pu and Pu–O shells based upon experimental work performed on copper catalysts [18].

of the sodalite cage structure would look much different than a bulk oxide. Several possibilities exist, including a $PuCl_3$-like pattern or plutonium interacting with the cage itself. The first coordination shell could be O, Al, Si, and/or other ions in the cage with the plutonium. XRD would not be able to detect any PuO_2 phases and may not show any change to the structure of the sodalite. Since we have not measured the EXAFS of plutonium occluded within the sodalite cage, it is possible that the EXAFS spectrum could be similar to that of extremely small PuO_2 particles that are external to the cage: less than 0.6 nm. From Fig. 8, N_{Pu-Pu} would be less than 3.5.

(4) *A range of PuO_2 particle sizes*. The most likely case is that there is a range of particle sizes and this is supported by TEM work [8] on materials of very similar nature to those in this work and indirectly by XRD, which was limited in predictive capability by the size of the quartz capillary used in the pattern acquisition. The distribution will strongly affect the results. In one scenario, there would be equal numbers of particles of every radius to some upper limit. Most of the plutonium (by number of atoms) will then be in the largest particles. The average coordination number will correspond to a particle size that is strongly weighted towards the largest particles. In fact, the smaller particles will make a nearly insignificant contribution to the average coordination number. Their number of atoms in the smaller particles would be very low, since the number of atoms is proportional to the cube of the radius. In careful XRD measurements, the peaks will have line shapes much like that of a large particle. Another scenario is that the plutonium is equally distributed in the small and large particles, which means that there are many more small particles than large. The measured coordination number will then be weighted more heavily toward the that of

the smallest particles. Careful XRD measurements may exhibit a somewhat unusual line shape with this distribution. As a result, if there is a wide size distribution, the size corresponding to the measured coordination number loses some meaning since EXAFS does not reveal information about the distribution. This behavior has not been supported by work on hot isostatically pressed samples, which are substantially similar in nature to the hot uniaxially pressed materials discussed in this work.

The results of fitting the data are shown in Table 5. The data for the ES-sodalite and DS-sodalite are averages over several samples and scans. For the ES-sodalite, N_{Pu-O} is nearly the same as for PuO_2, meaning that the first-shell oxygen cube is nearly filled in these samples. This finding, in itself, shows that very little, if any, plutonium resides in the sodalite cages or any other phase, as the plutonium in another phase would have a much different coordination environment than bulk PuO_2. Thus, an upper limit of less than ca. 5% is estimated for any plutonium not in a PuO_2-like structure (including that occluded in the sodalite cage). Any amount above this 5% limit should be visible in the spectra, were it present. The measured number of Pu–Pu next-nearest neighbors is less than for PuO_2. From fitting to an experimental reference/sample, N_{Pu-Pu} is 10.6 ± 0.4, which indicates an average particle size of 4.8 (+1.9/−1.1) nm from Fig. 8. Since TEM/XRD measurements imply a PuO_2 particle size centering at approximately 20 nm, there must be a wide particle size distribution in these samples, with a preponderance of the plutonium in small PuO_2 particles, as described implicitly in case 4, above.

For DS-sodalite, the picture is not as clear. Both N_{Pu-O} and N_{Pu-Pu} are significantly reduced from the bulk value. When the PuO_2 particles are small enough, there is not a complete oxygen cube around each plutonium atom, and N_{Pu-O} is reduced as a result. The Pu–O coordination number in the DS-sodalite is 35% lower than bulk PuO_2. Therefore the PuO_2 particle size is much smaller than for in ES-sodalite, i.e. N_{pu-Pu} is 6.2 ± 0.4. Both the Pu–O and Pu–Pu coordination numbers correspond to a particle size of 0.9 nm.

There is, however, an additional peak in the Fourier transform that does not appear in either the PuO_2 standard or the ES-sodalite cases. The extra peak implies that at least some plutonium is in an unknown second phase. A closer look reveals that the additional peak is due to high-Z atoms located at about 0.303 nm (see Fig. 9). The determination that it is a heavy element rather than a light element can be made from the envelope, or shape, of the $\chi(k)$ data. Nevertheless, it is not possible to identify what element is responsible for the peak. It is important to note that the shape of the plutonium–plutonium peak at 0.383 nm includes ripples to either side of the main peak. However, this alone does not account for the overall amplitude in the simulated fission-product salt case at ca. 0.3 nm distance. The addition of a heavy-element path at 0.303 ± 0.005 nm (see Table 5) results in a very good fit to the entire range (0.13–0.43 nm) for the k^1-weighted data and a very good fit to the range between 0.27 and 0.43 nm in the k^3-weighted case.

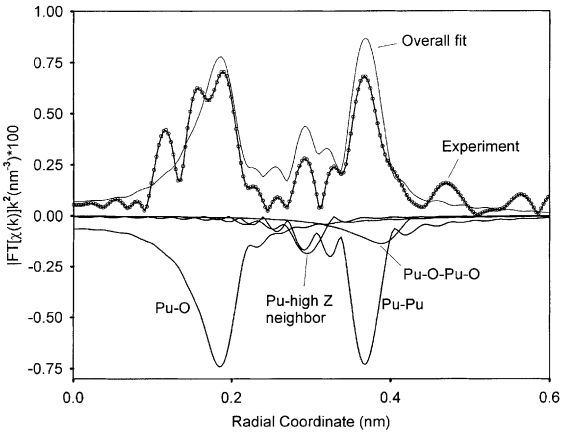

Fig. 9. Plot of the total Fourier transform contribution plus fit versus the contribution from the most significant individual paths/shells. The total Fourier transform and the fit are plotted as a positive set of values; the individual shell contributions of the fit are plotted as negative values to make them more clearly visible in this plot.

If the reduction to N_{Pu-O} is entirely due to the presence of other phases, then as much as 35% of the Pu could be present in those phases, which may include occlusion within sodalite cages. On the other hand, XRD measurements suggest that the DS PuO_2 particles are, in fact, smaller than the ES particles, so 35% seems like a rather large estimate of the plutonium not in PuO_2. In addition, N_{Pu-Pu} seems to be reduced by too much for complete oxygen cubes around each Pu atom to be likely. Therefore the most likely amount of plutonium not as PuO_2 would be less than 35%.

However, the presence of another phase indicates that a small fraction of the plutonium is not in a PuO_2-like phase. Therefore, the actual coordination numbers for the PuO_2 phase are larger than measured. Exactly how much depends on how much of the plutonium is tied up as PuO_2. A reasonable estimate based on the contribution to the overall fit by the heavy element path is that 85% of the plutonium is present as PuO_2. Under that assumption, the average PuO_2 particle size is 1.4 ± 0.2 nm. In addition, due to anharmonic effects discussed previously, the average size could be slightly larger. TEM/XRD measurements have shown that the PuO_2 particle size is closer to 2.0 nm, in reasonably good agreement with the EXAFS data.

7.1. Oxide versus oxychloride formation

With the conclusions drawn above, it is relevant to revisit the issue of plutonium oxide versus plutonium oxychloride formation. Reactions (1)–(4) suggested that oxychloride formation is preferred. However, it is a very well-established principle that a reaction that has a small equilibrium constant may be driven forward if one or more of the reaction products are removed or if its activity, if in solution, is reduced (LeChatelier's Principle). On this basis, we can write the reaction:

$$\begin{aligned} &2PuCl_3 + 3Li_2O + H_2O(g) \\ &\quad = 2PuO_2(c) + 6LiCl + H_2(g) \\ &\Delta_r G^\circ_{673\ K} = -304 kJ/mol;\ \ \Delta_r H^\circ_{673\ K} = -291\ kJ/mol, \end{aligned} \tag{5}$$

where the Li_2O is obtained by the hydrolysis of the LiCl component of the eutectic salt by the water present within the zeolite lattice at the time of salt/zeolite blending:

$$\begin{aligned} &H_2O(g) + 2LiCl = Li_2O + 2HCl(g) \\ &\Delta_r G^\circ_{673\ K} = -103.6\ kJ/mol; \\ &\Delta_r H^\circ_{673\ K} = 135\ kJ/mol\ (\text{on an LiCl basis}) \end{aligned} \tag{6}$$

that is driven to the right by the removal of Li_2O in reaction (5) and also the removal of HCl since this is far from a closed system in practice. As this reaction has been observed via differential scanning calorimetry to start occurring at a relatively low temperature ($\leqslant$673 K) in the equivalent uranium based experiment [20], we are considering the $\Delta_r G^\circ$ values at 673 K for this discussion. If we calculate the $\Delta_r G^\circ$ values for reactions (1)–(4) at 673 K, we obtain, respectively, 6.85 and −4.76, −25.6 and −87.9 kJ/mol by comparison. As one can see, if Li_2O is present, reaction (5) will progress in substantial preference to reactions (1)–(3) and even over reaction (4). Multicomponent equilibrium calculations indicate that only trace levels of Li_2O are necessary to make this possible as long as the HCl in the system is allowed to escape, as it was in this process. The net result is that the thermodynamic picture of this system is consistent with the preferential formation of oxide when the initial thermodynamic picture would predict that plutonium oxychloride would be the preferred species.

8. Summary

XANES/EXAFS techniques were used to determine the fate of plutonium within a sodalite/glass composite waste form in two cases: where the plutonium was alone in an LiCl/KCl matrix (ES-sodalite) and where simulated fission-product elements were added representive of the spent fuel electrometallurgical treatment process (DS-sodalite).

Results from SEM/TEM [8] analysis suggest that a significant amount of plutonium was tied up as oxide but could not indicate the degree to which the plutonium was either segregated in the oxide phase or located in the interior of the sodalite lattice. The XANES data clearly correspond to the Pu^{+4} oxidation state data in the ES-sodalite case, confirming the identity of the plutonium as strictly PuO_2. The EXAFS data also clearly indicate the disposition of the plutonium as PuO_2 in the case of the ES-sodalite, with crystallite sizes that indicate the plutonium is outside of the sodalite cage structure.

The EXAFS data for the DS-sodalite indicate the presence of a heavy-atom nearest neighbor and/or the possibility that the plutonium is incorporated within the sodalite lattice as well, for a phase that could account for up to 35% of the total plutonium in the extreme limit, with 15% being the most probable value when one factors in the heavy-atom nearest neighbor contribution. The remaining plutonium was present as a small PuO_2 particles, similar in size distribution to the ES-sodalite waste form but having a non-trivially smaller crystallite size (1.3 versus 4.8 nm). In the overall picture, the EXAFS/XANES findings indicate clearly that oxide is the preferred form of the plutonium in these waste forms albeit, with some partitioning of the plutonium into other phases in the DS-sodalite case where there are other species competing for the water present in the system.

Given the results of this experiment, the utility of the EXAFS/XANES technique is clearly indicated in unusual systems like the salt-loaded zeolites where atoms may be occluded within the latticework of the zeolite molecule and hidden from direct observation by more conventional SEM and TEM techniques. The XANES/EXAFS technique also provides a bulk view of the material, whereas SEM and TEM techniques are limited to sampling small areas. In cases where the species to be determined is unequivocally of one type and definitive size, such as the ES-sodalite case, the XANES/EXAFS technique is of unquestioned utility in putting to rest questions of plutonium deposition where no other technique can. However, in a case where one ends up with a mixed species, such as in the DS-sodalite case, and with a particle size that does not definitely preclude occlusion within the zeolite/sodalite lattice on a size consideration basis, the picture becomes less clear and requires tying the synchrotron technique to other means of determining species identity and/or size. In this light, higher resolution XRD techniques are being pursued for these materials to widen the conclusions that can be drawn by combining XANES/EXAFS techniques with other analytical methods. Nonetheless, the results of this investigation have shown that occlusion of the plutonium chloride species within the sodalite material is at

best limited and also allows us to draw some conclusions about the likely thermodynamic behavior of this system. This latter result is particularly important in terms of being able to optimize the overall waste form production process and to avoid processing cases that could give rise to an unacceptable waste form. In the end result, XANES/EXAFS and SEM/TEM/XRD techniques act to give us both sides of the same coin and provide a powerful means of characterizing waste form materials.

Acknowledgements

Thanks go out to the staff of laboratory G-118 (Z. Tomczuk, J. Heiberger), G-109 (R. Blomquist, L. Leibowitz) and to the staff of Argonne National Laboratory – West and their Analytical Chemistry Laboratory for the stock plutonium metal and supplied assay results. Thanks also go out to J.T. Vaughey for assistance in matters of X-ray crystallography. This work was supported by the US Department of Energy under Contract W-31-109-Eng-38. The synchrotron work was supported, in part, with Argonne National Laboratory Directed Research and Development funds to investigate the application of synchrotron techniques to actinide systems. Use of the Advanced Photon Source was supported by the US Department of Energy, Basic Energy Sciences, Office of Science (US DOE-BES-OS), under Contract No. W-31-109-Eng-38. The MRCAT beamlines are supported by the member institutions and the US DOE-BES-OS under Contracts DE-FG02-94ER45525 and DE-FG02-96ER45589.

References

[1] C. Pereira, M.C. Hash, M.A. Lewis, M.K. Richmann, JOM 49 (7) (1997) 34.
[2] M.A. Lewis, D.F. Fischer, L.J. Smith, J. Am. Ceram. Soc. 76 (11) (1993) 2826.
[3] S.D. Conradson, I. AlMahamid, D.L. Clark, N.J. Hess, E.A. Hudson, M.P. Neu, P.D. Palmer, W.H. Runde, C.D. Tait, Polyhedron 17 (11) (1998) 599.
[4] D.W. Breck, Zeolite Molecular Sieves – Structure Chemistry and Use, Krieger, Malabar, FL, 1974.
[5] C.U. Segre, N.E. Leyarovska, W.M. Lavender, P.W. Plag, A.S. King, A.J. Kropf, B.A. Bunker, K.M. Kemner, P. Dutta, R.S. Duran, J. Kaduk, in: P. Pianetta et al. (Eds.), The MRCAT Insertion Device Beamline at the Advance Photon Source, CP521, Synchrotron Radiation Instrumentation: 11th US National Conference, American Institute of Physics, New York, 2000, p. 419.
[6] O. Kubaschewski, C. Alcock, P.J. Spencer, Materials Thermochemistry, 2nd Ed., Pergamon, UK, 1993.
[7] HSC Chemistry for Windows 3.0, Outokumpu Research Oy, Pori, Finland, 1997.
[8] W. Sinkler, T.P. O'Holleran, S.M. Frank, M.K. Richmann, S.G. Johnson, Mater. Res. Soc. Symp. Proc. 608 (1999) 423.
[9] S.I. Zabinsky, J.J. Rehr, A.L. Ankudinov, R.C. Albers, M.J. Eller, Phys. Rev. B. 52 (4) (1995) 2995.
[10] A.L. Ankudinov, B. Ravel, J.J. Rehr, S.D. Conradson, Phys. Rev. B 58 (12) (1998) 7565.
[11] M. Newville, B. Ravel, D. Haskel, E.A. Stern, Y. Yacoby, Physica B 209 (1–4) (1995) 154.
[12] T.J. Ressler, J. Phys. (Paris) IV 7 (1997) C2-269.
[13] W.H. Zachariasen, Acta Crystallogr. 2 (1949) 388.
[14] G. Ferguson, Structure Reports for 1988 55A (1988) 144.
[15] J.H. Burns, J.R. Peterson, J.N. Stevenson, J. Inorg. Nucl. Chem. 37 (1975) 743.
[16] L.R. Morss, T. Fujino, J. Solid. State Chem. 72 (1988) 353.
[17] L.R. Morss, T. Fujino, J. Solid State Chem. 72 (1998) 338.
[18] B.S. Clausen, L. Gråbæk, H. Topsøe, L.B. Hansen, P. Stoltze, J.K. Nørskov, O.N. Nielsen, J. Catal. 141 (1993) 368.
[19] T. Shido, R. Prins, J. Phys. Chem. B 102 (1998) 8426.
[20] D. Lexa, L. Leibowitz, A.J. Kropf, J. Nucl. Mater. 279 (2000) 57.